Effect of Cloud–Radiation Feedback on the Climate of a General Circulation Model

J. SHUKLA AND Y. SUD

Goddard Laboratory for Atmospheric Sciences, NASA/Goddard Space Flight Center, Greenbelt, MD 20771

(Manuscript received 16 September 1980, in final form 9 July 1981)

ABSTRACT

The General Circulation Model (GCM) of the Goddard Laboratory for Atmospheric Sciences (GLAS) was integrated for 107 days starting from the initial conditions of 15 May. In this experiment the clouds dynamically generated by the model affect the radiative heating fields continuously. Starting from the initial conditions valid for day 76 of this run, another integration was made for 31 days in which the clouds were specified on certain grid points, remaining fixed during the period of integration. The spatial distribution of the fixed clouds was such that the aggregate cloud frequency for a vertical level and each latitude circle remained the same as in each control run, and the highest cloud frequency grid points were assigned the cloudiness of 100%. The 31-day mean simulation of the second run (fixed clouds) is compared with the last 31-day mean simulation of the first run to study the effects of cloud–radiation feedback on the mean monthly circulation, atmospheric energy cycle and the hydrological cycle, evaporation and precipitation and the local climate.

Results from these experiments show significant changes in the simulated large-scale dynamical circulation of the global model. Fixed clouds acting as zonally asymmetric radiative heat sources increase the generation of eddy available potential energy (EAPE) and its conversion to eddy kinetic energy. Generation of EAPE by net radiative heating increased by 50% (0.11 W m^{-2}) for the fixed cloud experiment. The increase due to the stationary component was much larger (~100%) but it was partially compensated by decrease due to the transient component. A substantial increase was found in the variances of the planetary-scale stationary waves and the medium-scale waves (wavenumber 6–10) of 2–7 day period. Although the sea surface temperatures were prescribed identically in both integrations, the changes in evaporation and precipitation were found to be much larger over the oceans compared to those over the land. We suspect that this happens because the ground temperature is determined by the model's heat balance at the earth's surface and therefore internal model feedbacks do not allow the hydrologic cycle over land to be very different between the fixed cloud run and the control run. Based on these calculations, we infer that cloud–radiation feedback is an important mechanism in the general circulation of the model atmosphere. It must be adequately parameterized in numerical experiments designed to simulate the mean climate and/or to examine the sensitivity of GCM's to changes in external boundary conditions or internal atmospheric constituents (such as aerosols and CO_2) and their feedback effects.

1. Introduction

The role of clouds in the atmospheric general circulation appears to be paradoxically dual. On the one hand, organized cloud ensembles owe their origin to large-scale dynamical forcing while, on the other hand, they provide one of the most important mechanisms of vertical redistribution of heat, moisture and momentum for the large scale. Clouds reflect the incoming solar radiation and thereby reduce the total solar energy available to the earth–atmosphere system. They also absorb and emit terrestrial radiation; thereby reducing the net outgoing thermal radiation. The role of clouds as agents of coupling between dynamical and hydrological processes has been a subject of extensive investigation. With the advent of GCM's there has been an increased interest in the parameterization of cloud–radiative feedback processes. In the pioneering general circulation work of Manabe and Holloway (1971), climatological zonally-averaged cloud distributions were specified. More recently, as a further simplification, Hunt (1978) reported the results of a numerical experiment in which zonally symmetric clouds were completely removed. In Hunt's studies the prescribed clouds had no zonal asymmetry. Therefore, the removal of clouds did not change the zonally averaged dynamical fields. This result is not surprising, particularly when Hunt's model did not have other asymmetric forcings such as land–sea contrast, interactive hydrology and snow/ice albedo feedback. However, since the zonally averaged clouds had a prescribed meridional structure, their removal did indeed change the mean meridional circulation.

Wetherald and Manabe (1980) have studied the response of a three-dimensional simplified model with idealized geography to changes in solar constant for fixed and variable cloud experiments. They

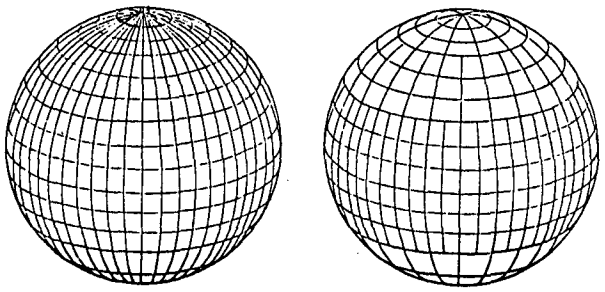

FIG. 1. Schematic representation of split grid structure of the model.

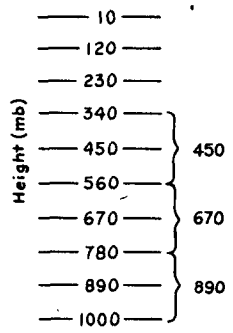

FIG. 2. Representation of strapped cloud from the model layers (pressures are nominal for P_s = 1000 mb).

found that the model response due to changes in the solar constant is not too different for the fixed and the variable cloud experiments. They attributed this to the compensation between changes in the incoming solar radiation and outgoing longwave radiation due to changes in the cloud amount and cloud height. It should be noted, however, that they examined only the zonally and globally averaged climate sensitivity to changes in the solar constant; they have not examined the regional changes in the mean climate due to fixed and variable clouds for the same value of solar constant.

One of the primary contentions of this paper is that the main differences between the fixed cloud and the variable cloud cases are produced by zonally asymmetric heating fields, and, therefore, zonal and global averaging will tend to show smaller response.

In recent years, there has been an increased interest in understanding the role of global cloudiness in determining the global albedo and its effect on net radiation balance of the earth–atmosphere system. This paper does not address this question because the problem of long time-averaged global mean climate is beyond the perview of this paper. It is well known that the dynamical circulation is the primary determinant of the horizontal, vertical and temporal distributions of cloudiness. Since the fluctuations of dynamical circulation can be affected by the radiative and hydrological effects of clouds, it is physically less realistic to treat them independently. Moreover, since the model integration was carried out only up to a season, we confined our study only to changes in the mean monthly circulation due to fixed and variable clouds. We have analyzed the differences between the two simulations, one with fixed clouds and the other with dynamical clouds (varying continuously in space and time). Whereas it is expected that continued absence or presence of a cloud cluster will significantly change the local hydrological cycle, persistent zonal asymmetry in the cloudiness field has been found to increase the eddy available potential energy (EAPE) and its conversion to eddy kinetic energy (EKE), and therefore the nature of the large-scale circulation.

The main dynamical effects of the fixed and the variable clouds are produced by changes in the generation of EAPE due to the altered heating field. Since EAPE is generated by correlation between heating and temperature, the magnitude of the effect will depend upon the way the clouds are prescribed in the fixed cloud experiment. Wetherald and

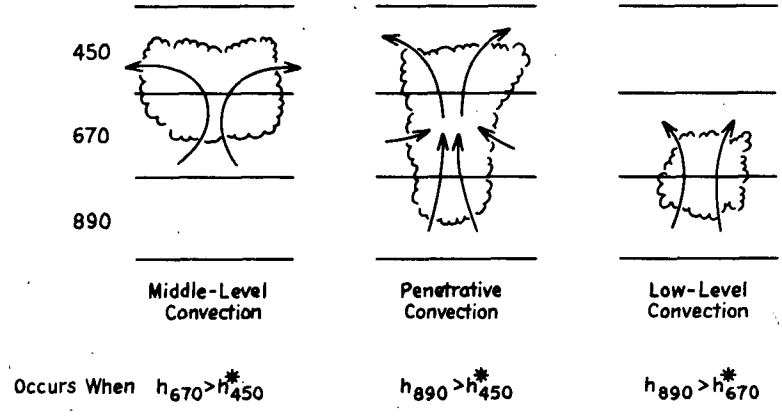

FIG. 3. Schematic representation of mid-level, penetrative and low-level convective clouds.

TABLE 1. Radiative properties of clouds in the GLAS model.

Cloud type	Layers*	Analogy	Optical thickness τc
Supersaturation	2	Ci	1
Supersaturation	3	Ci	2
Supersaturation	4	As	4
Supersaturation	5 or 6	As	6
Supersaturation	7 or 8 or 9	St	8
Penetrating convection	4–7 or 5–8 or 6–9	Cb	32
Mid-level convection	5 or 6	Ac	8
Low-level convection	7 or 8	Cu	16

* Layers are 110 mb thick, and layer 1 corresponds to interval between 10 and 120 mb.

Manabe (1980 and personal communication) chose 10 cloud fields from the control simulation and randomly introduced them at the appropriate time step. It is reasonable to assume that by doing so they did not drastically change the zonal asymmetry of the cloud field; however, random introduction of one of the 10 cloud fields could produce changes in the generation of EAPE. In this experiment, we have prescribed the cloudiness to be either zero or 100% at any grid point; this may appear to be an extreme case of longitudinal asymmetry. However, since the areas of 100% cloudiness are those where cloudiness was already maximum in the control (variable cloud) case, this may not be an unreasonable prescription. We have calculated the generation of EAPE due to radiative heating for both the experiments and present the results in Section 4.

2. The GLAS model

The GLAS GCM is a primitive equation model with a horizontal resolution of 4° latitude × 5° longitude. The grid is nonuniform near the poles and its horizontal resolution becomes 4 × 10° between latitudes 66 and 78° and 4 × 20° between latitudes 82 and 90°. A schematic diagram of the split grid is shown in Fig. 1.

The model has nine vertical levels in sigma coordinates. A detailed discussion of the model's hydrodynamics and physics may be found in Somerville *et al.* (1974). A more recent version of the model is discussed by Halem *et al.* (1979). The time-steps

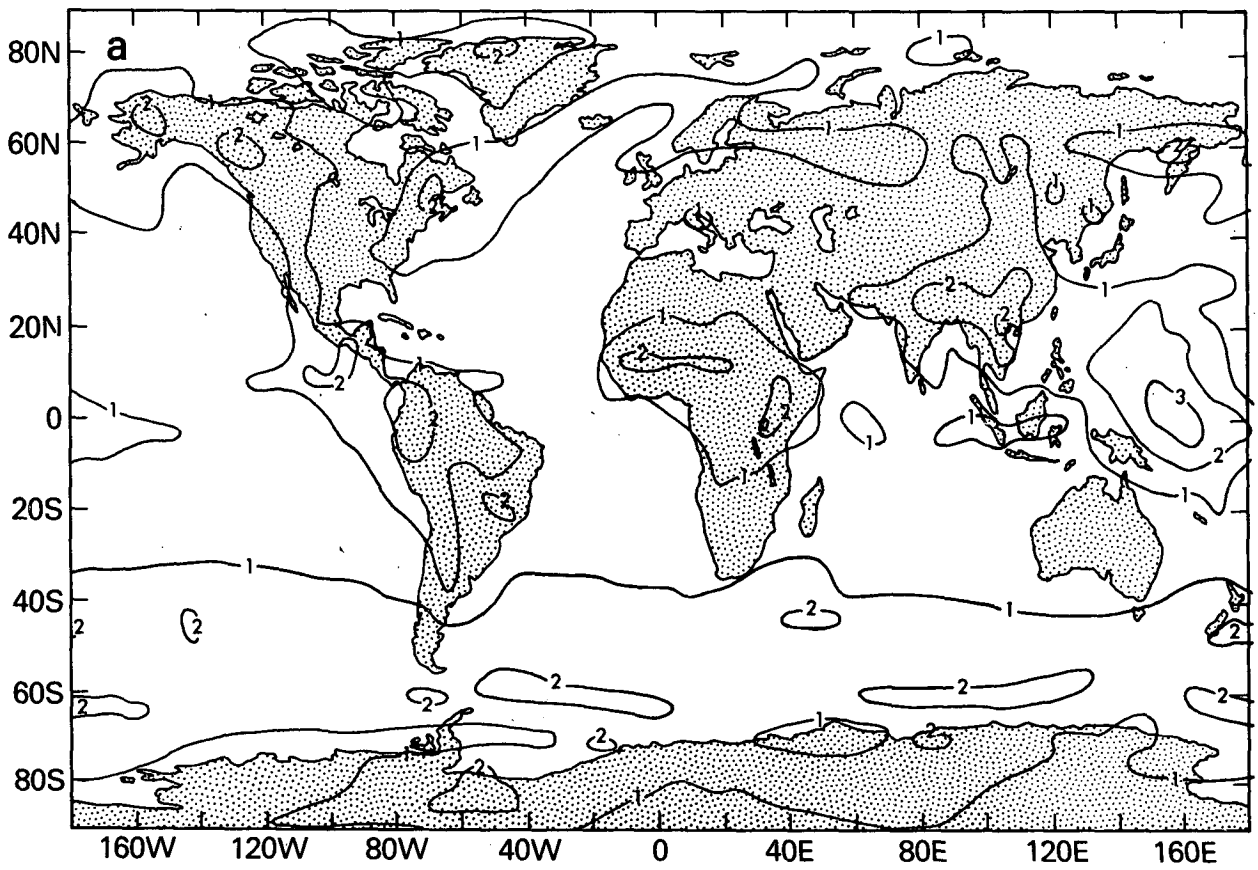

FIG. 4a. Cloudiness frequency (tenths) for the control run.

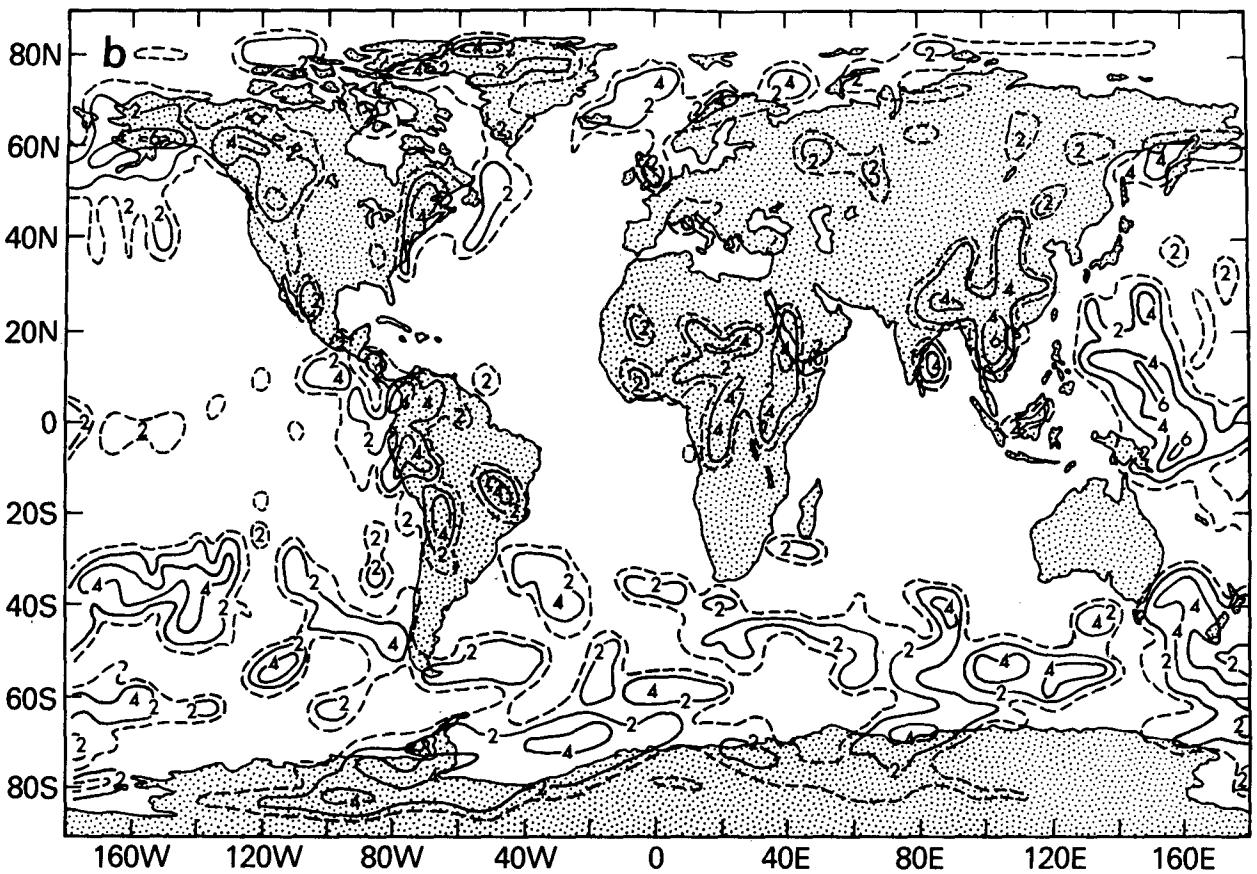

FIG. 4b. Vertically averaged cloudiness frequency (fixed cloud). Digits in parentheses represent range of values (on either side) in units of percentage: 0( )10(1)20(2)30(3)40(4)50(5)60(6)70(7)80(8)90(9)100.

for integrations are 10 min for hydrodynamics, 30 min for physics and 5 h for both the longwave and shortwave radiation. The instantaneous values of cloudiness at every fifth hour are used for calculating the shortwave and longwave radiative heating.

a. Cloud parameterization

The model generates four types of clouds. They occur sequentially. First, the mid-level, then deep, and then the low-level cumulus clouds are generated. These are followed by the calculation of supersaturation clouds. Each cloud modifies the environment at its sigma-level, and therefore affects the onset of subsequent clouds in the sequence. There are only three types of cumulus clouds to correspond to the Arakawa three-level model [Arakawa (1972)]. The adaptation of nine-level model to three-level cumulus parameterization is done by first limiting the cumulus clouds to the lowest six-levels of the GLAS model. Then, these six model layers are reduced to three cloud layers by strapping sets of two layers into one. The strapped layers are centered at 450, 670 and 890 mb (see Fig. 2). These three strapped layers are suitable for adaptation of the Arakawa three-level cumulus model, shown schematically in Fig. 3. Each type of cloud represents an ensemble distributed uniformly over the area of a grid cell whose effect can be statistically represented by a single entraining plume. A cumulus cloud appears between two levels if the moist static energy at the cloud base exceeds the moist (saturation) static energy at its top. For the deep convective clouds the moist static energy at the cloud base must be more than that at the levels penetrated. The supersaturation clouds can appear at any level if the specific humidity at that level exceeds the saturation specific humidity. Sequentially, the supersaturation clouds are calculated after the cumulus clouds. A detailed discussion of the cloud parameterizations is given in Arakawa (1972) and Helfand (1979).

b. Radiative effects of model clouds

Model clouds can be generated in any of the nine vertical model levels spaced uniformly in pressure from 10 mb at the top level to surface pressure at the bottom of level 9. The model may generate "supersaturation" clouds at any level from 1 to 9; low-level convective clouds in levels 7 or 8, "mid-level

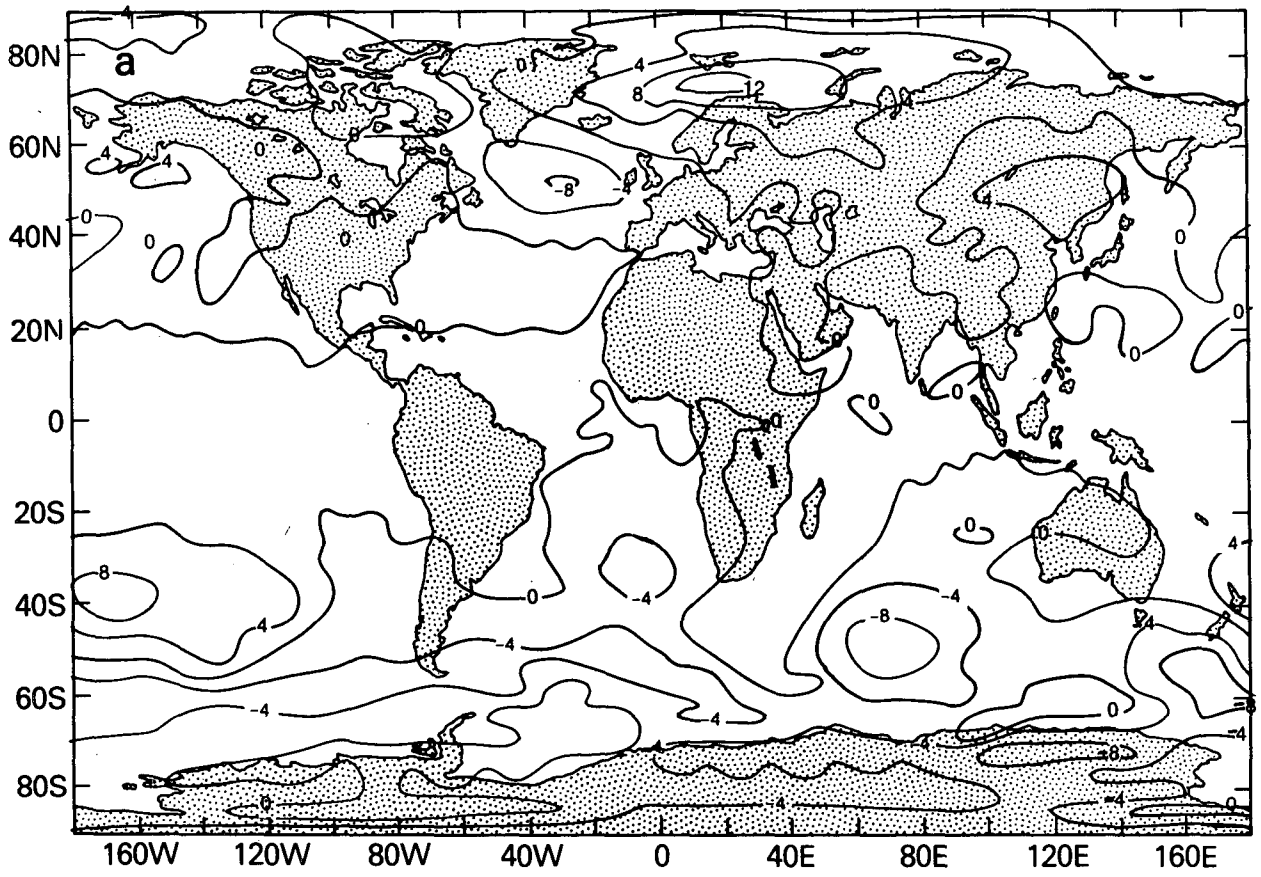

FIG. 5a. Differences in the mean monthly sea-level pressure (mb) (fixed cloud–control).

convective" clouds in levels 5 or 6, or "penetrating convective clouds" in any four consecutive levels between 4 and 9. The presence of any cloud type at any level implies that the cloud occupies the whole area of the horizontal grid element. The solar optical thickness τ_c, which is one of the intrinsic radiative parameters depending on cloud type and cloud level, is given in Table 1.

The treatment of cloud effects on shortwave radiation is described by Lacis and Hansen (1974). Single-scatter albedo a_c and the asymmetry factor g_c of the phase function for scattering by the cloud droplets are given constant values of $a_c = 1$ and $g_c = 0.85$. The absorption of solar radiation within a given cloud layer is determined by combining τ_c, a_c and g_c with the spectrally dependent parameters due to the amount of water vapor in the layer, and the two-stream radiative transfer model is applied allowing for interaction between the cloud layers and the underlying surface.

The treatment of cloud effects on longwave radiation is extremely simple. If a cloud appears at any grid point, irrespective of its height and type, it is considered as a blackbody, covering the entire horizontal area of the grid element. We recognize that this is a questionable assumption; however, the assumption is made for both experiments in an identical way. In GCM sensitivity experiments, it is implicitly assumed that although control simulations have certain shortcomings, the calculated differences are still reasonable approximations to correct response.

3. Experiment

The control run was started from the observed initial conditions of 15 May 1974, and integrated for 107 days. Monthly means for the last 31 days, representing simulated August, were analyzed for this study. In this run, clouds were continuously generated according to the model parameterization, and therefore they were varying in space and time. Then starting from day 76 of the control run, the model was again integrated for 31 days during which cloudiness for radiation–cloud interaction was spatially prescribed and was invariant in space and time. This run is referred to as the "fixed cloud run."

The spatial distribution of clouds in the fixed run was chosen to be such that the aggregate cloudiness frequency over all the grid points at each vertical

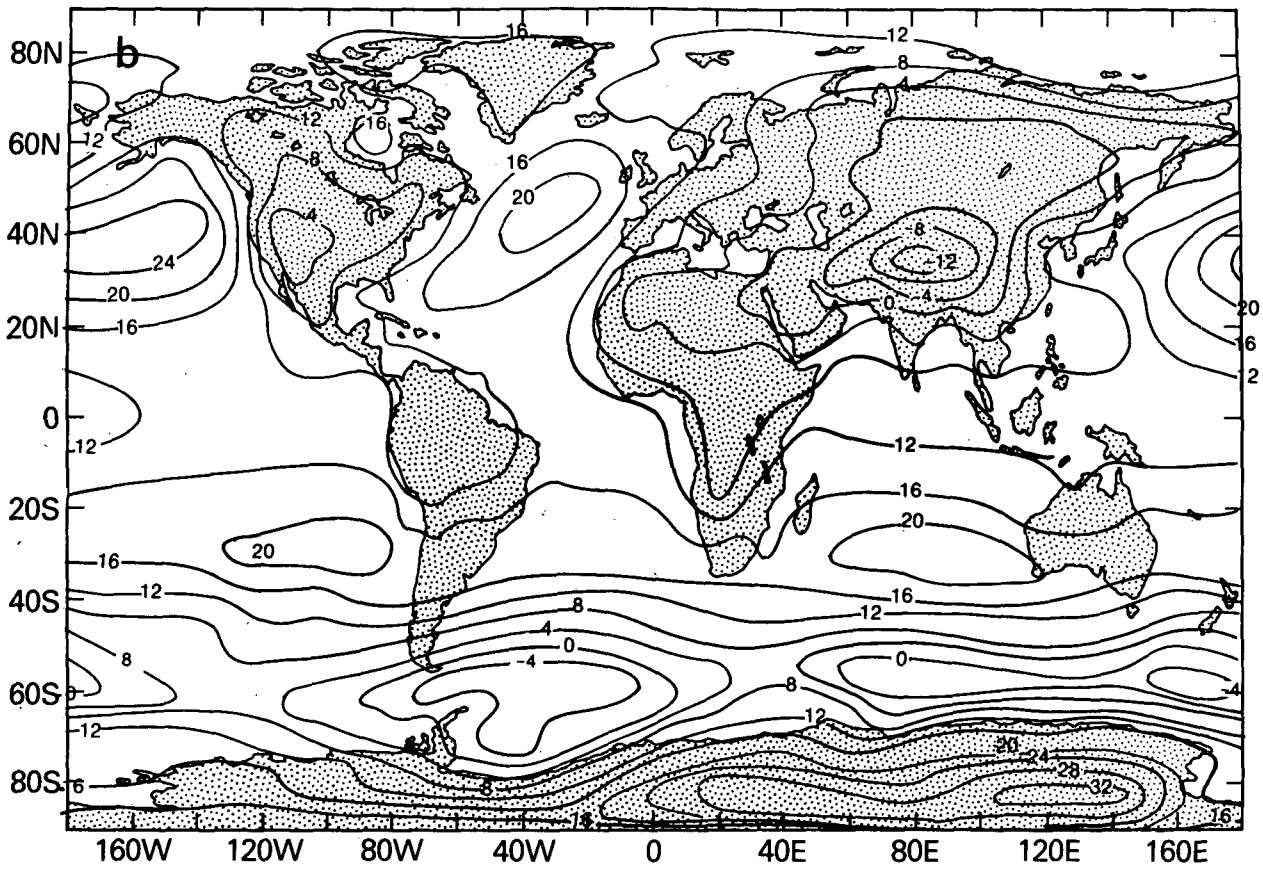

FIG. 5b. Mean monthly sea level pressure (−1000 mb) field generated in the control run.

level and each latitude circle remained nearly the same for the control and the fixed cloud run. The procedure for obtaining the fixed cloud data set consisted of defining a number $N = \sum_{i=1}^{72} f_i$, where f_i was the cloudiness frequency with a value between 0 and 1 at any grid point i. N was then rounded off to an integer and equals the number of grid cells which have clouds in the fixed cloud experiment. Such N grid cells were chosen in the order of highest f_i in the control run. This condition implied that the cloud frequency in a grid cell was either 0 (no cloud) or 100% (permanent cloud) in the fixed cloud case. Clouds were prescribed on grid cells which produced the highest cloud frequency in the control case. It may be emphasized that the statistically averaged cloudiness fields were very similar in both the cases. The only difference in the two runs was that in the fixed cloud case, the cloudiness for radiative cloud interaction was held constant for the period of integration.

Figs. 4a and 4b show the vertically averaged cloudiness frequency for the control and the fixed cloud runs, respectively. The cloud frequency indicates the percentage occurrences of all types of clouds during a one-month period sampled at the time of cloud–radiation interaction (every 5 h). It should be pointed out that normally cloudiness maps are not vertically averaged, and, therefore, comparison of Figs. 4a and 4b with observed or other model simulated clouds cannot be done in the present form. In the context of the present study, we considered it to be more appropriate to display vertically averaged cloud maps.

4. Analysis of results

Various meteorological fields have been analyzed to study the difference between the two runs. We do not know how well the model had equilibrated to the initial perturbations in the field of cloudiness; however, since the sea surface temperature is prescribed, and since the time scale of large-scale cloudiness is comparable to the time scale of fast changing internal dynamics, 31-day integration can be considered to be adequate for this purpose. For more definitive results, longer integrations should be performed. In order to examine the significance of these differences, the natural variability of the model's July

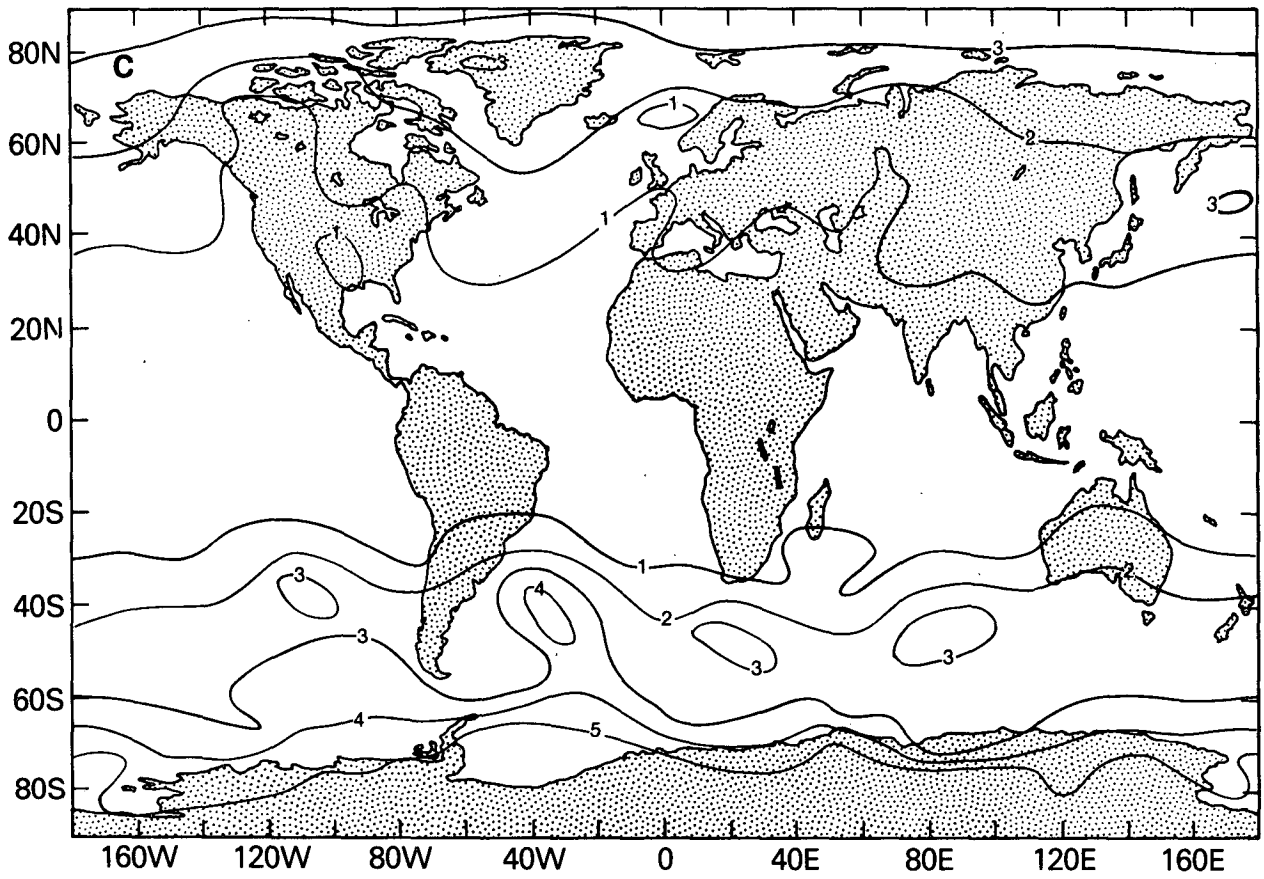

FIG. 5c. Natural variability (mb) of sea level pressure for the simulated month of July.

simulations is also presented. The natural variability of the model is based on the control run and three predictability experiments in which only the initial wind fields at each of the nine model levels were randomly perturbed with a Gaussian error field having a standard deviation of 3 m s^{-1}. For each predictability experiment, the model was integrated for 45 days, and the monthly means for the last 31 days were used to calculate the natural variability of the model. It is assumed that the standard deviation (with Bessel correction) among the four runs (one control and three predictability runs) is a measure of the natural variability of the model.

a. Sea level pressure (SLP) fields and 500 mb geopotential height field

Fig. 5a shows the difference in the 31-day mean sea level pressure (SLP) between the control and the fixed cloud run, and Fig. 5b shows the corresponding mean SLP for the control run. Fig. 5c shows the natural variability of the model for SLP. Fig. 5a shows that the differences are 2–3 times the model variability. Maximum differences of 4–12 mb at about 50°N are to be compared to maximum model variability of 3 mb. Similarly, at 40°S the maximum differences of 4–8 mb occur around the subtropical highs. There does not appear to be any direct association between regions of cloudiness and the sea level pressure anomalies. It should be pointed out that the differences in SLP reflect the changes in large-scale dynamical circulation which may be forced by the differences in hydrological cycles of the model simulations, which was indeed very different in two runs.

Fig. 6a shows the differences in 500 mb geopotential height fields between the fixed cloud and control runs. Large differences are noticed in the latitude belt of 40–60°S. This is perhaps due to the combined effects of baroclinicity, which is maximum in this latitude belt (winter circulation), and the generation of EAPE due to large longitudinal asymmetry of the fixed cloudiness field at this latitude. Large differences also are seen in this field at 40–60°N. In the Northern Hemisphere (summer circulation) baroclinicity is relatively weak but zonally asymmetric heating in the fixed cloud run would be more because of larger solar flux. The

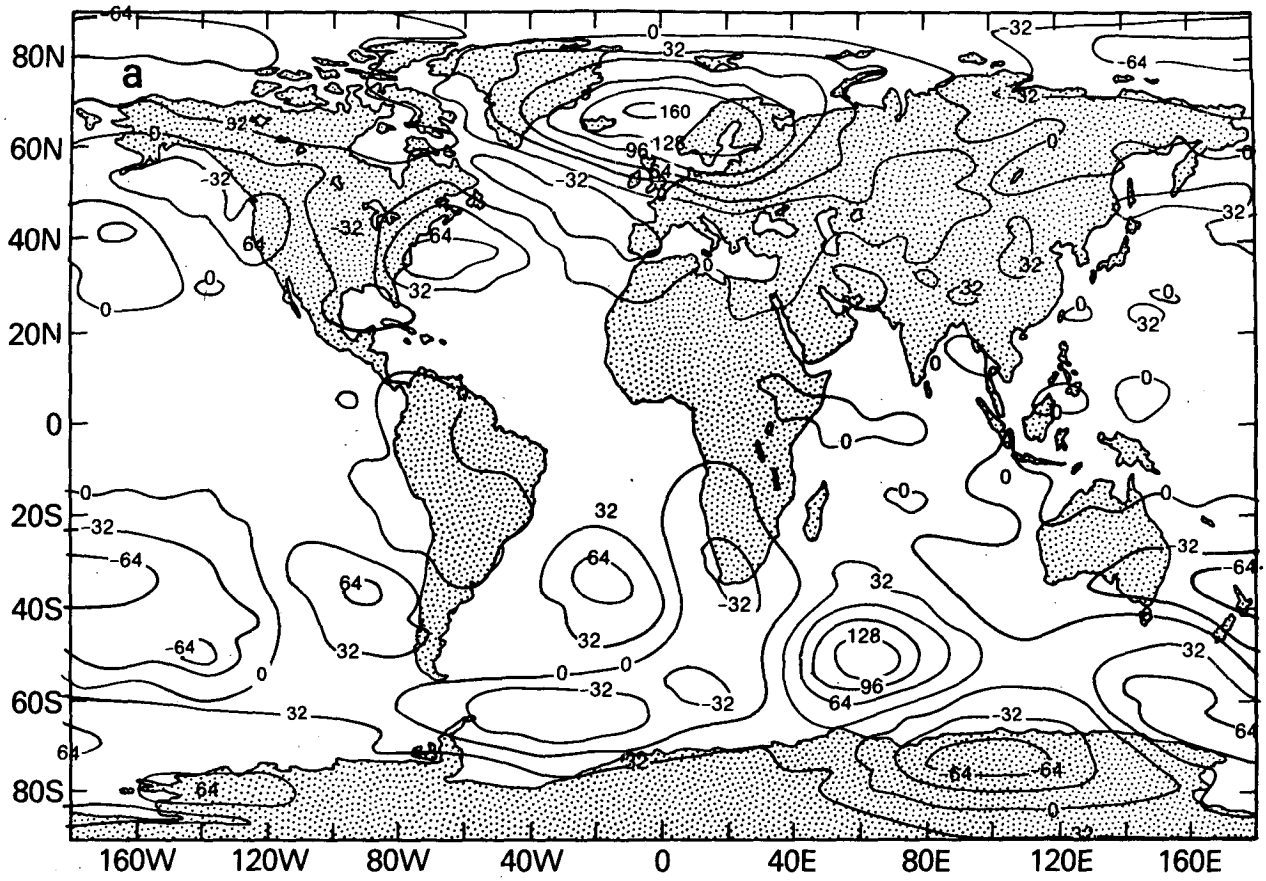

FIG. 6a. Differences in the mean monthly 500 mb geopotential height (meters) (fixed cloud–control).

differences in these fields are also 2–3 times the model's natural variability [Fig. 6b].

b. Atmospheric energetics

Figs. 7a and 7b show the energy cycle of the Southern Hemisphere and the Northern Hemisphere, respectively. Each figure has four sections, each of which gives the energy cycle for the control run, the fixed cloud run, their differences, and the corresponding model variability. In the Southern Hemisphere, the model variability of all the energy conversion [EAPE to EKE, ZAPE (zonal available potential energy) to EAPE, ZKE (zonal kinetic energy) to EKE and ZAPE to ZKE] are larger than their corresponding differences between the two runs. This shows that, due to the combined effects of large baroclinic growth rates and small solar flux, the natural variability of a mean monthly simulation in the baroclinically active winter circulation is larger than the differences in these energy conversions created by zonally asymmetric fixed cloudiness. However, the situation in the Northern Hemisphere is quite different. For the control run in the Northern Hemisphere (summer circulation), baroclinic energy conversion from EAPE to EKE is not as strong as its counterpart in the Southern Hemisphere. This, of course, is due to the reduction of vigorous baroclinically unstable wave activity during summer. However, the differences in the atmospheric energy cycle between the control run and the fixed cloud run are comparatively larger than the natural variability of the model. For example, the differences in EAPE and EKE for the Northern Hemisphere are more than four times the natural variability. The presence of fixed clouds is equivalent to an asymmetric heat source which enhances the generation of EAPE and its conversion to EKE. The changes in other energy conversions are not so significant.

Table 2 shows the generation of EAPE due to diabatic heating by stationary and transient components in the Northern Hemisphere. Radiative damping of EAPE has been reduced from -0.31 to -0.20 W m^{-2}, which means that generation of EAPE has increased by 0.11 W m^{-2}. The increase

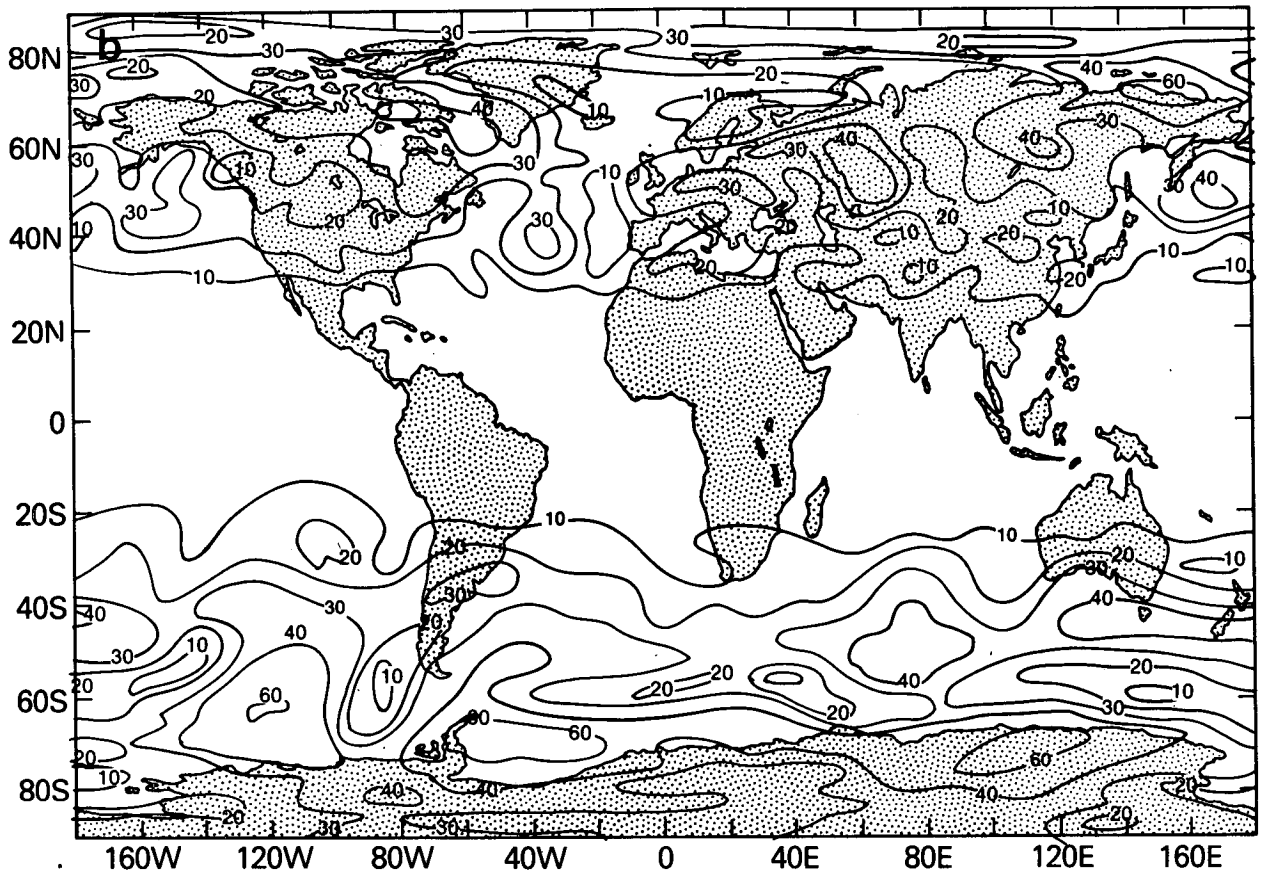

FIG. 6b. Natural variability of 500 mb geopotential height (meters) for the simulated month of July.

for the stationary component alone is 0.38 W m^{-2}; however, it is compensated by a decrease of 0.27 W m^{-2} in generation due to transient components. Generation of EAPE due to total diabatic heating shows a large increase from 2.0 to 2.39 W m^{-2}. This suggests that although increase in generation of EAPE due to radiative processes alone was only 0.11 W m^{-2}, the model circulation produced positive feedbacks to increase the total generation of EAPE by 0.39 W m^{-2}.

The differences in the energy cycles of the two runs suggest a mechanism through which cloud–radiation interaction can provide significant feedbacks to the dynamical circulation which, in turn, gives rise to significantly different regional circulations.

c. *Evaporation, precipitation and sensible heat flux*

Figs. 8a and 8b show the difference between the fixed cloud and the control run for 31 days mean evaporation and precipitation, respectively. Large changes in the evaporation and precipitation fields are seen over the tropical and subtropical western Pacific Ocean. These differences are also seen in the baroclinically active Southern (winter) Hemisphere. This is possible because the sea surface temperature is prescribed over the oceans, and any change in the net radiative flux at the surface, due to prescribed cloudiness, does not have a feedback on the ocean surface temperature. If the net effect of prescribed cloudiness is to cool (heat) the interior atmosphere above the ocean surface, it occurs without a corresponding change in the ocean surface temperature, and therefore increases (decreases) the moist convective fluxes of heat and moisture to the atmosphere. Furthermore, because the precipitation is affected by local monthly mean evaporation, any local changes in evaporation produce corresponding changes in precipitation.

Another important mechanism which affects the precipitation in the fixed cloud run is the change in the vertical profiles of moist static energy in the atmosphere, which affects the onset and intensity of the convective precipitation in this model. The vertical profile of moist static energy is clearly

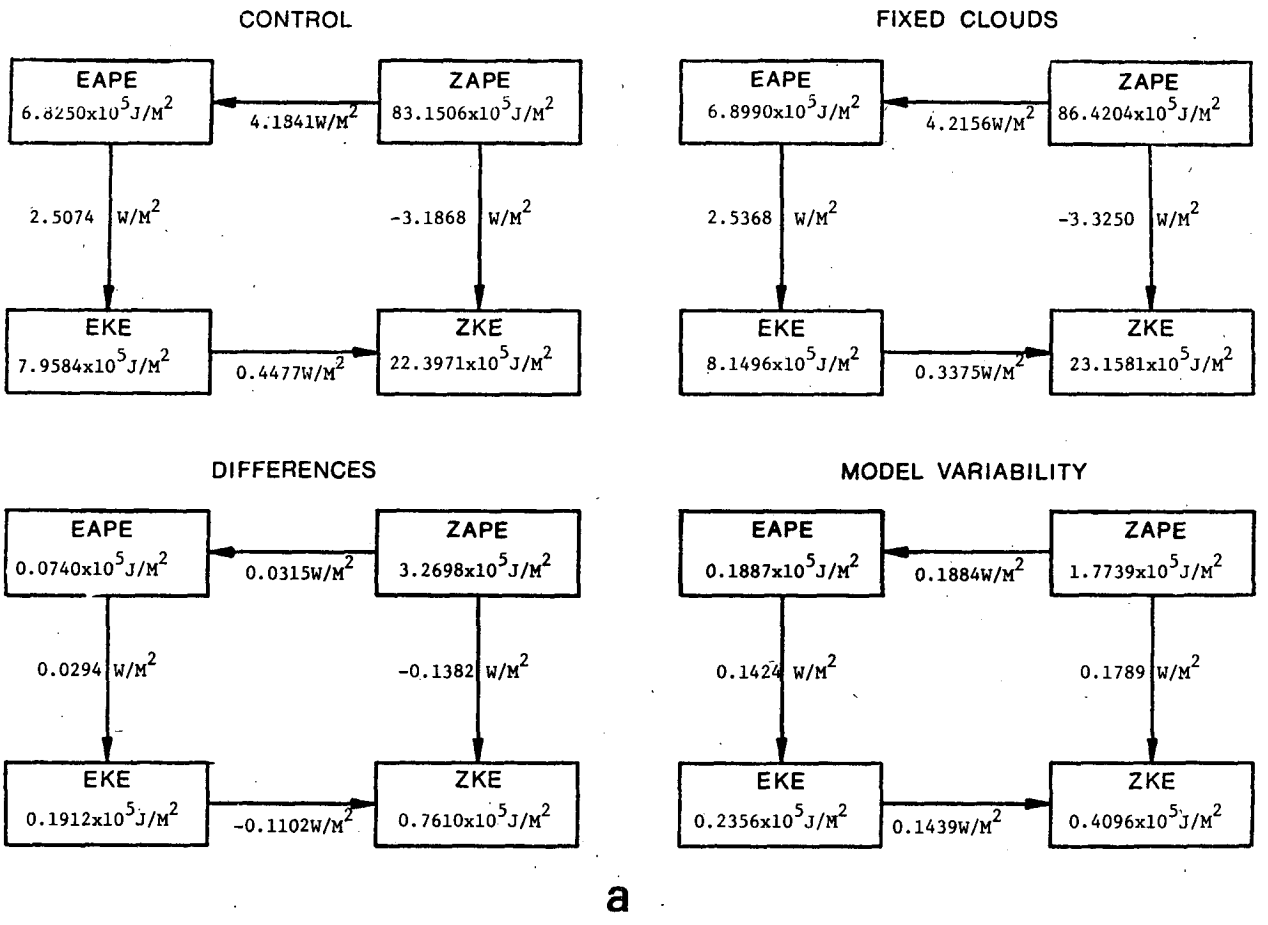

FIG. 7a. Southern Hemisphere energy cycle for control, fixed cloud, differences, and model variability.

affected by asymmetric radiative heating in the fixed cloud run. We are indeed struck by such large changes in evaporation and precipitation over the oceans, because it is generally believed that numerical models with fixed sea surface temperature may not be very sensitive to the prescribed cloudiness field. The results of these simulations, on the contrary, point out a large impact of cloudiness on the evaporative fluxes and precipitation over oceans. On the other hand, the changes in these fields over land are not so large because the ground temperature, a prognostic variable in the model, can adjust to anomalous changes in the radiative heat fluxes. It should be remarked, however, that these effects may depend upon the details of the parameterization of model physics in general and moist convective parameterization in particular.

TABLE 2. Generation of eddy available potential energy (W m^{-2}) for Northern Hemisphere.

	Net radiative heating		Total diabetic heating	
	Control	Fixed clouds	Control	Fixed clouds
Stationary	−0.20	0.18	1.41	2.02
Transient	−0.11	−0.38	0.59	0.37
Total	−0.31	−0.20	2.00	2.39

Figs. 9a and 9b show the zonal rms differences in the evaporation and precipitation fields, respectively, for the control and the fixed cloud runs, and also, for comparison, the average of the zonal rms difference between the control run and each of the three predictability runs. Between the latitudes 10°S–35°N, the differences between the control and the fixed cloud runs are twice as large as the differences between the control and the predictability runs. It should be pointed out, however, that the local variability is much larger than that inferred from the zonal averages, and that variability over oceans is larger than that over the land.

Fig. 8c shows a digitized map of sensible heat flux

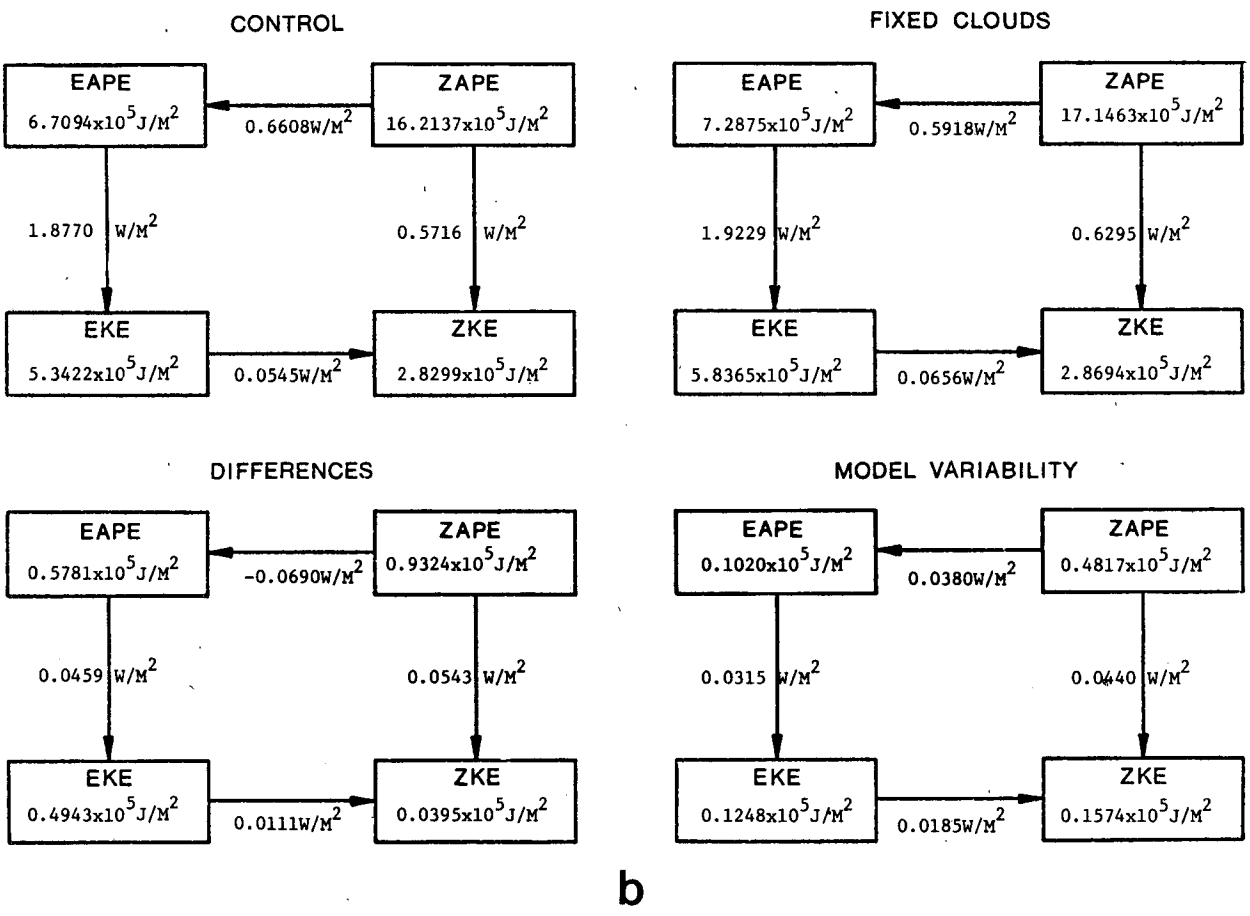

FIG. 7b. Northern Hemisphere energy cycle for control, fixed cloud, differences, and model variability.

difference between the fixed cloud run and the control run. It is seen that the sensible heat flux to the atmosphere is generally reduced in those regions where cloudiness was prescribed in the fixed cloud run. This reduction is more systematic over the oceans than over the land. Since the ocean temperature is prescribed identically in both the runs, the reduction of sensible heat flux may be associated with the increased warming of the air overlying the ocean due to increased downward radiation from the cloud base.

Thus, the fixed clouds cause a small decrease in the sensible heat flux, and a large increase in evaporation and precipitation. The two effects are not mutually inconsistent because, for small changes in the surface wind speed, the changes in the sensible heat flux are associated with changes in the air temperature immediately overlying the earth's surface, whereas the intensity of moist convection and its associated precipitation depend on the vertical temperature gradient between the lower layers and the interior of the atmosphere. An enhanced moist convective activity provides a mechanism for removing the lower level moisture, drying the environment by subsidence and therefore increasing the evaporation from a prescribed sea surface temperature.

TABLE 3. Variance (m^2) of 500 mb geopotential height field at 50°N for different wavenumber and frequency ranges.* Control run numbers are above those of fixed cloud run.

Period (days)	Wavenumber 1–5	6–10	11–36	Total
15.5	609	175	32	816
	608	142	36	786
3.9–7.8	131	85	42	258
	119	99	38	256
2.2–3.1	10	8	14	32
	9	8	13	30
Stationary	1611	326	37	1974
	2470	176	46	2692

* Total (stationary + transient) variance: control = 3080.0, fixed cloud = 3764.0.

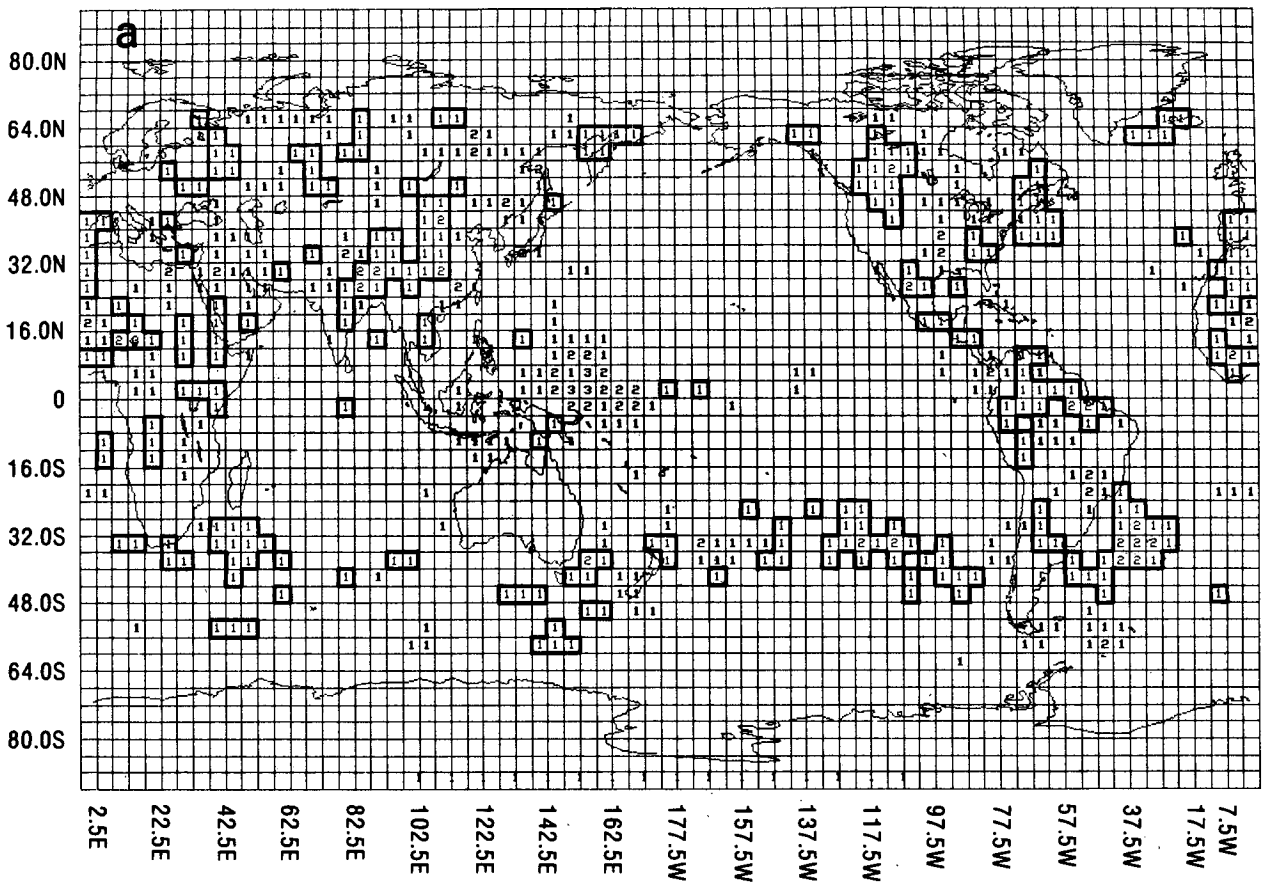

FIG. 8a. Differences in evaporation (fixed cloud–control). Thin numbers inside the bounded regions have negative sign. Digits in parentheses represent the range of values (on either side) in units of 0.1 mm day^{-1}: 0( )0.5(1)1.5(2)2.5(3)3.5(4)4.5(5)5.5(6)6.5(7)7.5(8)-8.5(9)9.5 or more.

d. Space–time spectral analysis

We have carried out a space–time spectral analysis, as described by Straus and Shukla (1980), of the 500 mb geopotential height field at two selected latitudes. We show the variance as a function of wavenumber and frequency at 50°N in Table 3. Since the natural variability of the Southern Hemispheric winter circulation was found to be too large (Section 5), we have not presented the space–time spectra for the Southern Hemisphere. Table 3 shows that the total variance in the fixed cloud run has increased by 22%. Most of the increase is due to the increase in the variance of planetary-scale (wavenumber 1–5) stationary waves. The variances of the medium-scale (wavenumber 6–10) stationary waves and low-frequency (period 15.5 days) waves have decreased. We do not have a measure of the natural variability of the variances to estimate its significance. Nonetheless, it is remarkable to note that the variance of high wavenumbers (6–10) and medium frequencies (period 4–8 days) has increased by ~17%. These results suggest that the presence of zonally asymmetric forcing in the fixed cloudiness run amplifies the perturbations whose horizontal scale corresponds to wavenumber 6–10 and time period corresponds to 4–8 days. Since these space and time scales correspond closely to the preferred scales of baroclinically unstable perturbations, this suggests a possible relationship between asym-

FIG. 8b. Differences in precipitation (fixed cloud–control). Thin numbers inside the bounded regions have negative sign. Digits in brackets represent the range of values (on either side) in units of 0.1 mm day^{-1}: 0( )0.5(1)1.5(2)2.5(3)3.5(4)4.5(5)5.5(6)6.5(7)7.5(8)-8.5(9)9.5 or more.

FIG. 8c. Differences in sensible heat flux at the surface (fixed cloud–control). Thin numbers inside the bounded regions have negative sign. Digits in brackets represent the range of values (on either side) in units of cal cm^{-2} day^{-1}: 0( )10(1)20(2)50(3)70(4)90(5)110(6)-130(7)150(8)170(9)190 or more.

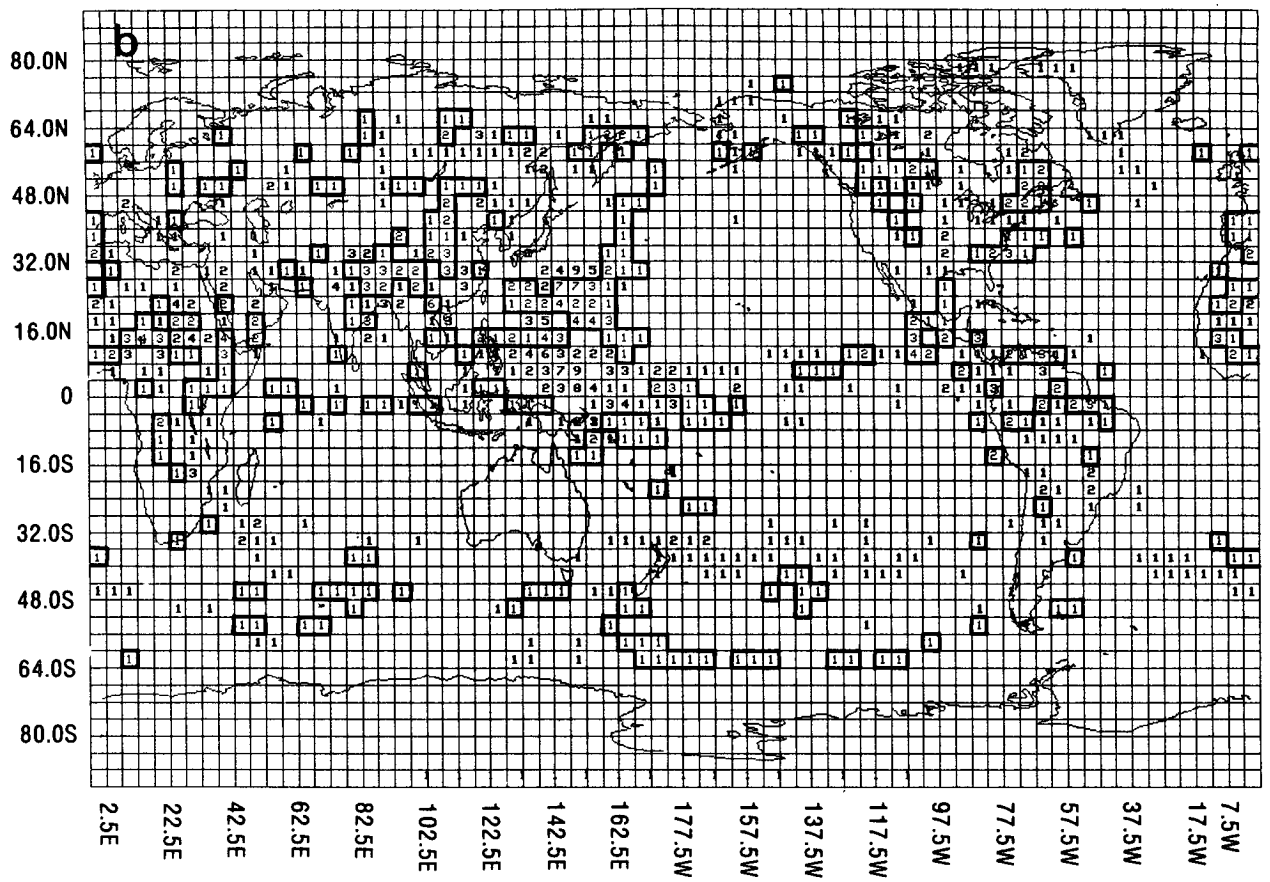
b
80.0N
64.0N
48.0N
32.0N
16.0N
0
16.0S
32.0S
48.0S
64.0S
80.0S
2.5E
22.5E
42.5E
62.5E
82.5E
102.5E
122.5E
142.5E
162.5E
177.5W
157.5W
137.5W
117.5W
97.5W
77.5W
57.5W
37.5W
17.5W
7.5W

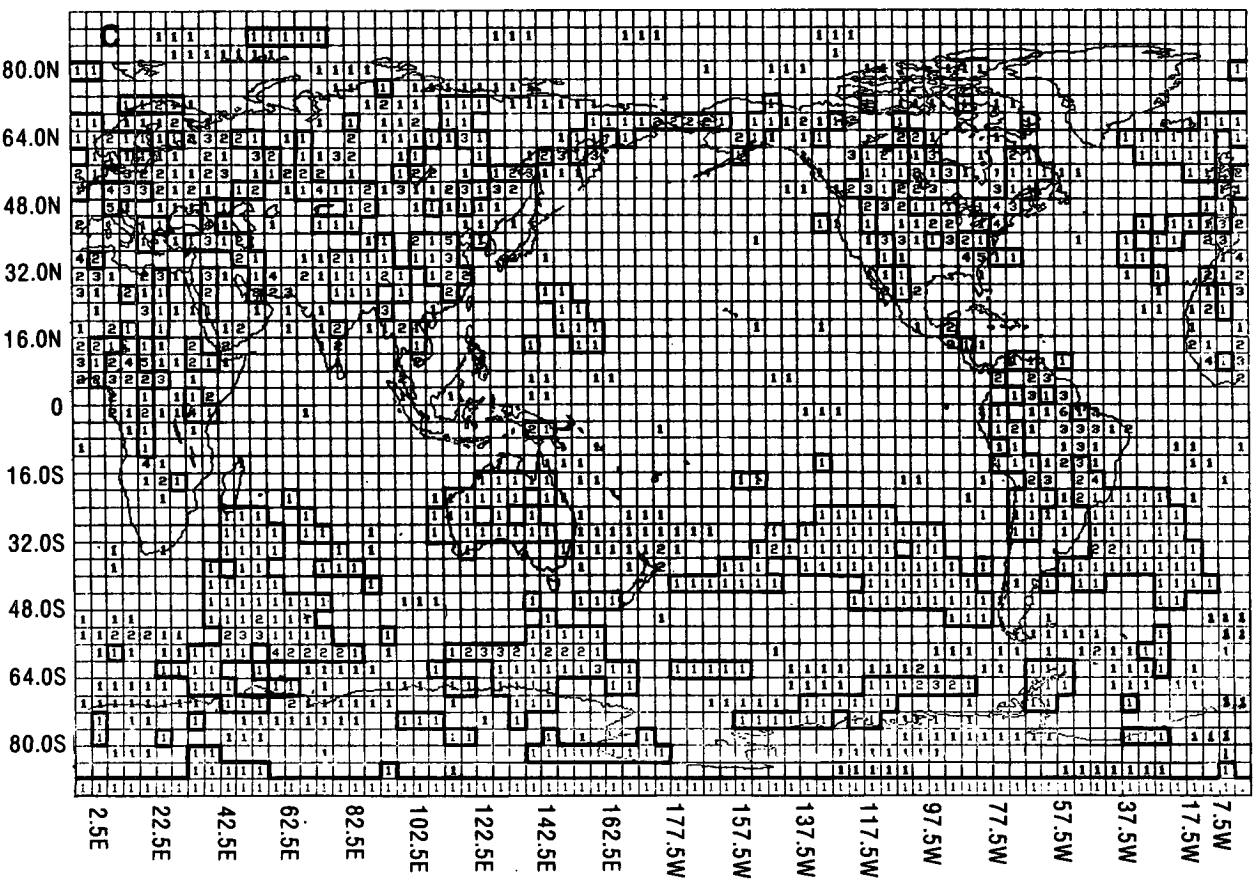
c
80.0N
64.0N
48.0N
32.0N
16.0N
0
16.0S
32.0S
48.0S
64.0S
80.0S
2.5E
22.5E
42.5E
62.5E
82.5E
102.5E
122.5E
142.5E
162.5E
177.5W
157.5W
137.5W
117.5W
97.5W
77.5W
57.5W
37.5W
17.5W
7.5W

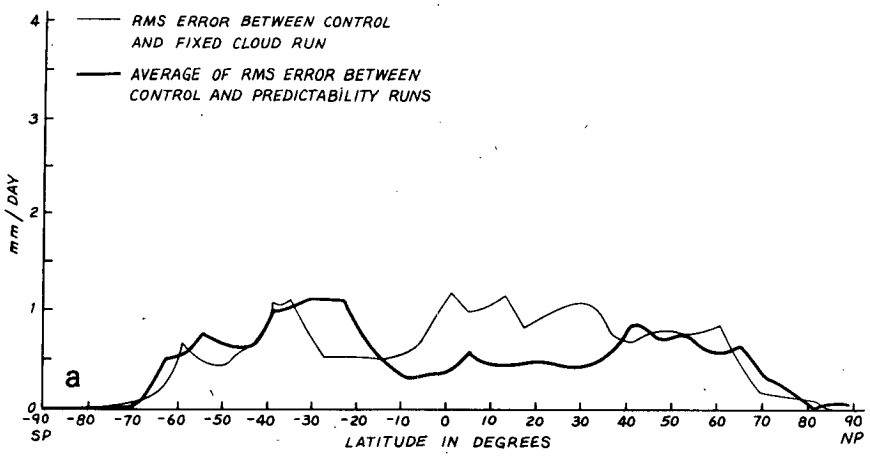

FIG. 9a. Zonally averaged ms difference of monthly mean evaporation between control and fixed cloud runs, and their averages for control and each predictability run.

metric radiative forcing and intensity of baroclinic wave activity.

Since the mean radiative–dynamical equilibrium of the atmosphere's heat budget is maintained by the joint contributions of heat fluxes due to eddy activity and the zonally averaged mean circulations, it is reasonable to expect a reduction in the intensity of the zonally averaged Hadley circulation to accompany an increase in the intensity of the eddy activity. We have examined the intensity of the Hadley cell in both integrations and found that it was indeed weaker in the fixed cloud run compared to the control run. Since we do not have an estimate of the natural variability of the Hadley cell, we cannot comment on the significance of these differences. It was also seen that the intensity of the Ferrel cell was reduced in the fixed cloud case. This is not inconsistent with the fact that although high wavenumber, medium-frequency waves were stronger, stationary and low-frequency medium waves were much weaker.

e. Heat balance of the atmosphere

Table 4 gives the global radiation balance for the two runs. First, in the fixed cloud run the global albedo is lower than that of the control run. This is due to smaller spatial coverage of the clouds in the fixed cloud run. The cloud clustering is an artifact of the procedure used in preparing the fixed clouds data set. Reduced planetary albedo should result in larger absorption of the shortwave radiation, which should be balanced by an increase in the longwave flux. However, in these model runs, an increase of 0.008 cal cm^{-2} min^{-1} in the solar absorption is accompanied by an increase of only 0.003 cal cm^{-2}

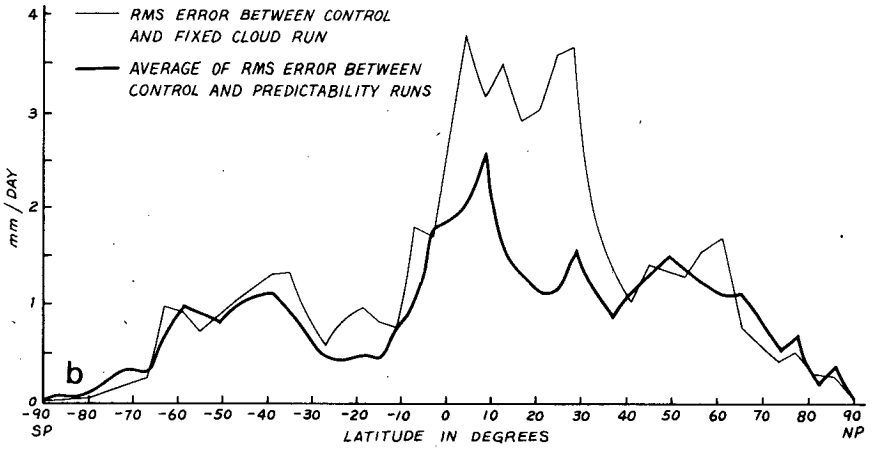

FIG. 9b. Zonally averaged rms difference of monthly mean precipitation between control and fixed cloud runs, and their averages for control and each predictability run.

TABLE 4a. Global radiation budget of the earth–atmosphere system (cal cm^{-2} min^{-1})

	Solar radiation			Longwave radiations (outgoing)	Net radiation balance
	Incoming	Absorbed	Albedo		
Control	0.488	0.334	0.315	0.287	0.047
Fixed clouds	0.488	0.342	0.299	0.290	0.052
Difference	0.000	0.008	−0.016	0.003	0.005

TABLE 4b. Heat balance at surface of the earth (cal cm^{-2} min^{-1})

	Net incoming solar radiation flux at surface	Net upward longwave radiation flux at surface	Net upward sensible heat flux	Net atmospheric heating by condensation*	Net surface balance
Control	0.262	0.077	0.048	0.101	0.035
Fixed clouds	0.270	0.077	0.048	0.103	0.042
Difference	0.008	0.000	0.000	0.002	0.006

* This is approximated by net evaporation.

min^{-1} in the outgoing longwave radiation. This is so because the sea surface temperature in this model does not respond to changes in the net solar flux absorbed by the oceans. Changes in other radiation fields are negligibly small.

f. Radiation balance at the top of the atmosphere

The net radiation balance at the top of the atmosphere is shown in Figs. 10a and 10b for the two runs. The radiation balance is noisy for the fixed cloud

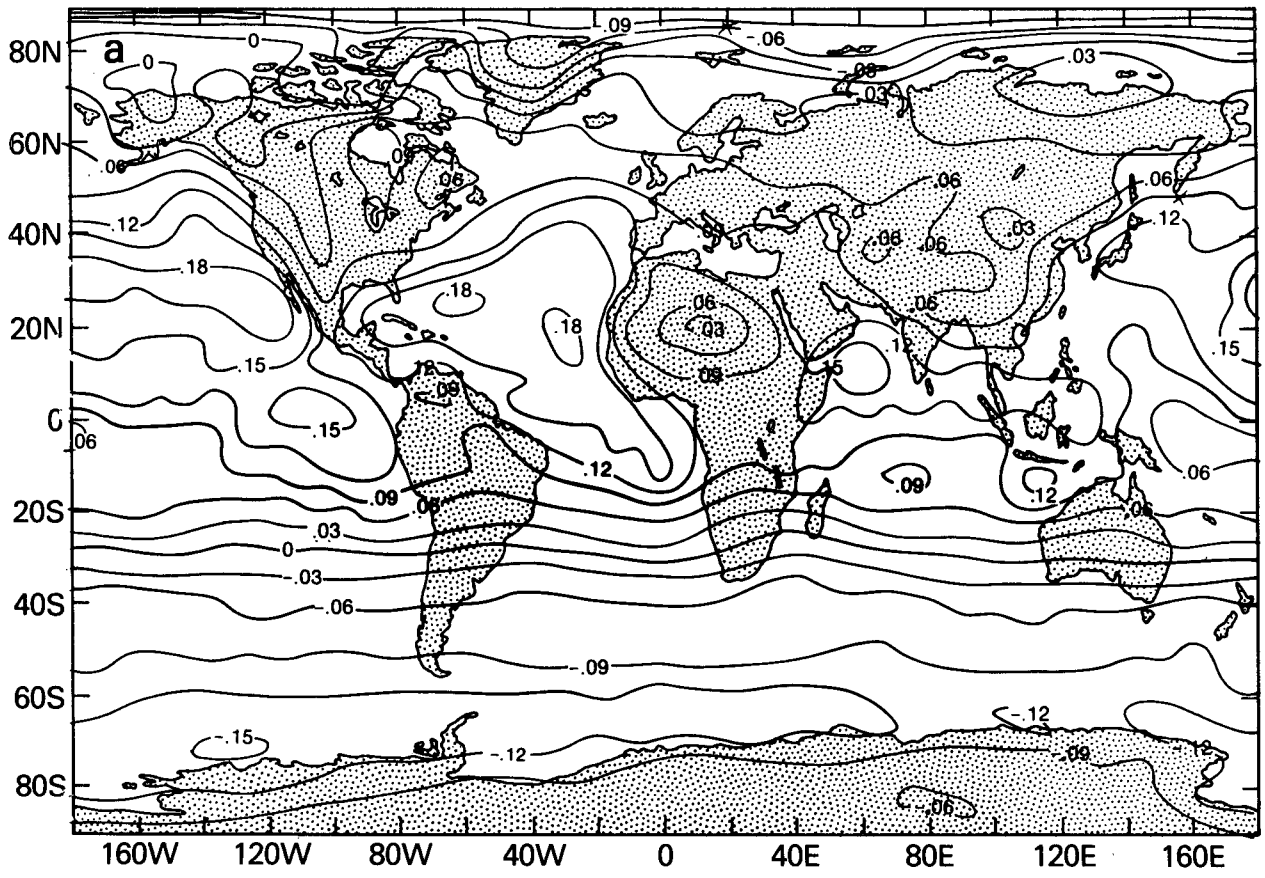

FIG. 10a. Radiation balance at the top of the atmosphere in cal cm^{-2} min^{-1} for the control run.

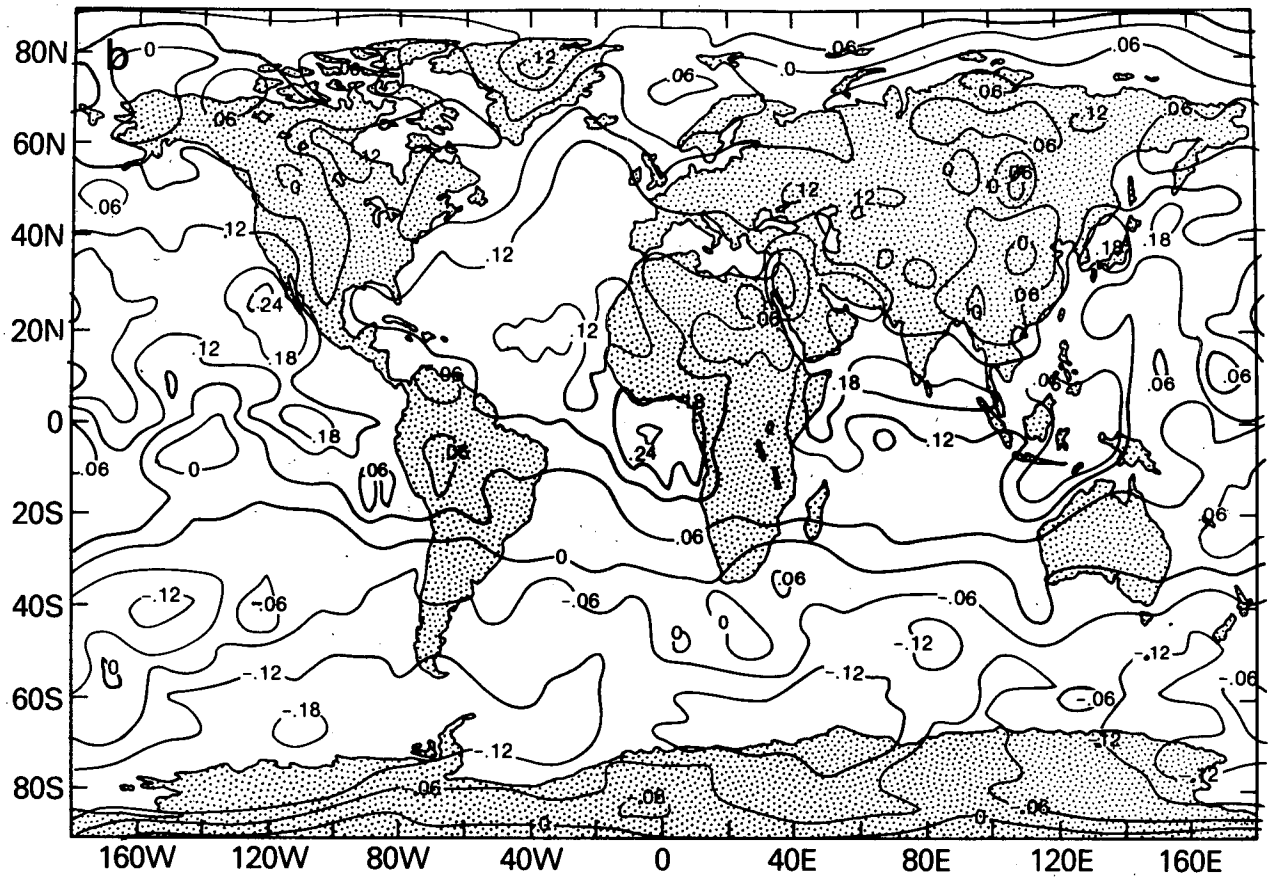

FIG. 10b. Radiation balance at the top of the atmosphere in cal cm^{-2} min^{-1} for the fixed cloud run.

run. The zonal structure corresponds to the zonal distribution of prescribed clouds. In the Atlantic Ocean at 30°N, the clouds are nonexistent in the fixed cloud run. Therefore, larger amounts of solar energy sinks at the ocean surface and the net radiation balance at the top is less than the control case. In the southern Pacific at 40°S, greater cloudiness in the fixed cloud run gives about twice the negative radiation balance, (-0.06 cal cm^{-2} min^{-1}) in the control case. These results emphasize the fact that the net radiation balance at the top of the atmosphere is not a very useful parameter to diagnose climate variability because it merely represents an outcome of a multitude of physical and dynamical processes operating underneath, and it cannot distinguish their relative contributions.

5. Conclusion

The monthly mean climatology of the GLAS GCM is significantly different in the fixed cloud run compared to the control run. In the control run, the clouds are generated dynamically, and therefore their radiative effects vary continuously in space and time. In the fixed cloud run, however, for the calculation of radiative effects the cloudiness field is initially prescribed and then held constant for the whole period of integration. Since the prescribed cloudiness varies geographically, the net radiative effects of the fixed clouds introduce a stationary thermal forcing with complex vertical structure. It is found that, in the fixed cloud run, the generation of eddy available potential energy and its conversion to eddy kinetic energy is larger than that of the control run. The variance of cyclone-scale transient waves and planetary-scale stationary waves also are found to be larger in the fixed cloud run. There are some significant changes in the large-scale dynamical circulation as evidenced from the fields of sea level pressure and geopotential height field at 500 mb.

Pronounced changes are also found in the local hydrological cycle (evaporation and precipitation) and these changes are predominant over the oceans where sea surface temperature was prescribed. Evaporation and precipitation increases over the Northern Hemispheric tropical oceans. Sensible heat flux to the atmosphere decreases in the regions of fixed cloudiness. It should be pointed out, however, that these effects may also strongly depend on the parameterizations of moist convection and the

treatment of radiative effects of clouds. For example, in the case of moist convective adjustment, the prescribed sea surface temperature will have a greater influence, and even though the prescribed cloudiness may tend to change the temperature at any level, the convection adjustment will act so as to bring it back to its mean value determined by sea surface temperature. This may result in a larger difference in local evaporation and precipitation, but it may not substantially change the large-scale circulation because the atmospheric temperature changes will be very small.

This study suggests that the processes of cloud–radiation feedback are important in determining the regional characteristics of the general circulation of the model atmosphere. These processes should be adequately parameterized for a realistic interpretation of predictability and sensitivity studies carried out with general circulation models.

Although it is well understood that the zonally asymmetric thermal forcing (heat sources and sinks) plays an important role in the dynamics of stationary and transient components of the general circulation, the contribution of radiation toward the total asymmetric thermal forcing is generally considered to be insignificant. This study suggests that changes in the radiative forcing, through cloud–radiation interaction, can produce changes in the hydrologic cycle, which in turn can produce substantial changes in the total thermal forcing and the dynamical circulation.

Acknowledgments. The authors wish to thank Dr. Milton Halem and Dr. G. Herman for many useful comments on the original manuscript. We also wish to thank Dr. R. T. Wetherald and Prof. W. R. Kuhn for their comments and suggestions on the earlier version of the manuscript. The authors particularly wish to thank Mr. E. Sabatino for his help with computer graphics and Miss Debbie Boyer, Miss Karen DeHenzel and Miss Laura Rumburg for their help with typing and drafting.

REFERENCES

Arakawa, A., 1972: Design of the UCLA atmospheric general circulation model. Tech. Rep. No. 7, Dep. of Meteorology, University of California, Los Angeles, 116 pp.

Halem, M., J. Shukla, Y. Mintz, Man-li Wu, R. Godbole, G. Herman and Y. Sud, 1979: Comparisons of observed seasonal climate features with a winter and summer numerical simulation produced with the GLAS general circulation model. Report of the JOC Study Conf. on Climatic Models: Intercomparison and Sensitivity Studies. *GARP Publ. Series*, WMO, Geneva, No. 22, 207–253.

Hunt, B. G., 1978: On the general circulation of the atmosphere without clouds. *Quart. J. Roy. Meteor. Soc.*, **104**, 91–102.

Helfand, H. M., 1979: The effect of cumulus friction on the simulation of a January Hadley circulation by the GLAS model of the general circulation. *J. Atmos. Sci.*, **36**, 1827–1843.

Lacis, A. A., and J. E. Hansen, 1974: A parameterization for the absorption of solar radiation in the earth's atmosphere. *J. Atmos. Sci.*, **31**, 118–133.

Manabe, S., and J. L. Holloway, Jr., 1971: Simulation of climate by a global general circulation model, 1, Hydrological cycle and heat balance. *Mon. Wea. Rev.*, **99**, 335–369.

Somerville, R. C. J., P. Stone, M. Halem, E. Hansen, J. S. Hogan, L. M. Druyan, G. Russell, A. A. Lacis, W. J. Quirk and J. Tenenbaum, 1974: The GISS model of the global atmosphere. *J. Atmos. Sci.*, **31**, 84–117.

Straus, D. M., and J. Shukla, 1980: Space-time spectral structure of the geopotential height of a GLAS general circulation model and a comparison to the atmosphere. *J. Atmos. Sci.*, **38**, 902–917.

Wetherald, R. T., and S. Manabe, 1980: Cloud cover and climate sensitivity. *J. Atmos. Sci.*, **37**, 1485–1510.